Pt nanoparticles with enhanced deaminase-like activity: example of oxidative deamination of 5-hydroxymethylfurfurylamine and glutamic acid.

Antoine Lancien[a], Egon Heuson[b], Franck Dumeignil[b], Ivaldo Itabaiana Jr[b], Renato Froidevaux*[a] and Robert Wojcieszak*[a]

[a] Dr Antoine Lancien, Prof. Renato Froidevaux Department : UMRT BioEcoAgro 1158 Institution: Univ. Lille, INRAE, Univ. Liège, UPJV, JUNIA, Univ. Artois, Univ. Littoral Côte d'Opale, ICV-Institute Charles Viollette F-59000 Lille (France) E-mail: antoine.lancien.etu@univ-lille.fr, renato.froidevaux@univ-lille.fr

[b] Dr Egon Heuson, Prof. Franck Dumeignil, Prof. Ivaldo Itabaiana Jr, Dr Robert Wojcieszak Department: Unité de Catalyse et Chimie du Solide, UMR CNRS 8181 Institution : Univ. Lille, CNRS, Centrale Lille, Univ. Artois F-59000 Lille (France)

E-mail : egon.heuson@centralelille.fr, franck.dumeignil@univ-lille.fr, robert.wojcieszak@univ-lille.fr

[c] Prof. Ivaldo Itabaiana Jr Department of Biochemical Engineering, School of Chemistry, Federal University of Rio de Janeiro, 21941910, Rio de Janeiro, Brazil, ivaldo@eq.ufrj.br

Abstract: Oxidative deamination is part of the metabolic pathways of amino acid oxidase and glutamate dehydrogenase enzymes, and enables obtaining *α*-keto acid from amino compound with ammonia as a by-product. This work presents the utilization of Pt-based catalyst composed of small platinum nanoparticles supported on industrial silica support (Pt/SiO_2). This nanozyme was tested in the oxidative deamination reaction of two amino compounds: *5*-hydroxymethylfurfurylamine (HMFA) to 5-hydroxymethylfurfural (HMF) and glutamic acid (GA) to *α*-ketoglutaric acid (KGA). This paper outlines the use of Pt nanozymes with deaminase-like activity. We showed the ability of this nanozymes to be selective and active in liquid phase oxidative deamination of HMFA and glutamic acid in a 6 to 9 pH range at 60°C under atmospheric pressure. Pt/SiO_2 nanozyme actually plays as a deaminase mimic with high HMFA conversion (60%) and cumulative yield to the corresponding desaminated keto compounds (67%).

Introduction

The oxidation of amino acids is a crucial step in the metabolism of these molecules. Oxidation kinetics using different oxidants in various media have been largely studied. It was shown that, generally, amino acids undergo oxidative deamination and decarboxylation [1-5]. Recently, an ortho-naphthoquinone-catalyzed oxidative deamination process was developed for the first time [6]. Authors reported, that O_2 and water serve as oxidant and nucleophile. In the case of aerobic deamination reaction, the mechanism is believed to occur *via* a ketimine formation between ortho-naphthoquinones and amines. The second step is the prototropic rearrangement and finally hydrolysis by water. This mechanism mimics the oxidative deamination of amino acids, which occurs in the human body by liver and kidneys [6].

Nanozymes have attracted much attention due to their relatively low cost, enhanced stability, and various enzyme-like activities [7]. Compared to enzymes, thermally activated nanozymes possess several advantages including a temperature-regulated activity and the possibility of using various green oxidants such as H_2O_2, molecular oxygen or air. Moreover, very often, higher activity can be achieved as compared to the corresponding enzymes. In addition, the stability of nanozymes is much better, as they are more prone to resist to poisoning and to

the effect of reaction co-products formation; further their recycling is greatly facilitated. Up to now, several nanomaterials with enzyme-like activities have been discovered. The most emblematic ones with a peroxidase-like activity are iron oxide (Fe_3O_4) nanoparticles [8-9], gold nanoparticles [10] and graphene oxide (GO) nanosheets [11]. Some authors also demonstrated that Pt and Pd nanoparticles as well as some reducible oxides such as CeO_2 and MnO_2 have inherent catalase (CAT) and super-oxide dismutase (SOD)-mimic abilities [12-13]. Especially small Au nanoparticles catalyzed the oxidation of glucose to gluconic, as glucose oxidase (GOx) mimics [14]. Mugesh and co-workers [15], reported that V_2O_5 nanowires behaves as a glutathione peroxidase (GPx) mimic.
Reductive deamination of glutamic acid was already reported (Scheme 1) using Pt catalyst [16].

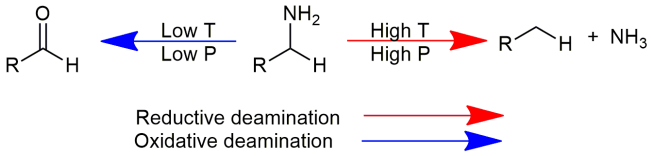

Scheme 1. Schematics of the possible deamination reactions on Pt catalysts.

Authors presented a two-step process to convert glutamic acid into dimethyl glutarate using Pt nanoparticles. Supported platinum nanoparticles were identified as the most efficient ones. They enabled high yields of dimethyl glutarate (> 70%) depending on the support nature (C, ZrO_2, TiO_2). The authors stated that the key of this excellent catalytic performance relies in the presence of metal support interactions, and especially between metal and the support acid sites with a moderate strength (both of the Brønsted and Lewis type). However, such good performances were obtained under relatively harsh conditions (225 °C and 30 bar H_2) [16]. Recently Jiang group [17] reported on chemo-enzymatic synthesis of α-keto acid using Pt supported on metal organic frameworks and immobilized L-amino acid oxidase (LAAO) in the synthesis of indol 3-pyruvic acid from L-tryptophan. The 99.7% yield was obtained for chemo-enzymatic catalyst, which was much higher then 41% observed in the case of free LAAO [17].
To the best of our knowledge, there is no work so far dealing with the oxidative deamination of amino acids using heterogeneous catalysts. In the present work, we report the application of nanozymes comprising Pt nanoparticles supported on SiO_2 for the oxidative deamination of two important amino compounds: *5*-hydroxymethylfurfurylamine (HMFA) and glutamic acid (GA). We showed that such a Pt/SiO_2 nanozyme actually plays as a deaminase mimic with high HMFA conversion and yield to the corresponding desaminated keto compounds.
Results and Discussion
Figure 1-left shows a TEM image of the prepared Pt/SiO_2 sample. A very high dispersion of Pt nanoparticles was obtained even with the relatively high metal loading of 6.3 wt.% (ICP). TEM analysis further showed that no agglomeration of Pt nanoparticles with a rather narrow particles' size distribution (Figure 1a) and an average particles' size of 1.8 nm.

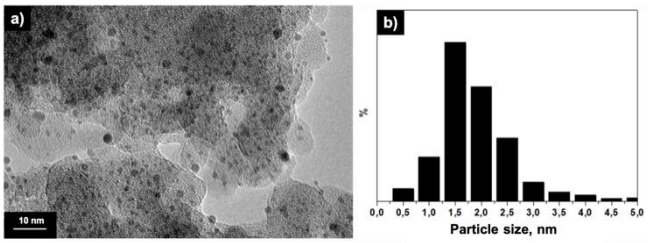

Figure 1. TEM image of the Pt/SiO_2 nanozyme catalyst (a) and particle size distribution (b).

The Pt particles' size was also determined by hydrogen chemisorption at 35 °C. The quantity of hydrogen adsorbed was quantified assuming that i) spillover of hydrogen is negligible, ii) the stoichiometry of the adsorption is 1:1, and iii) there is no multilayer adsorption (physisorption). The H_2 chemisorption derived average Pt particles' size was estimated at 1.6 nm (vs. 1.8 from TEM) with a dispersion ca. 70 %. H_2-TPD analysis was also performed to identify the different hydrogen species adsorbed on the Pt/SiO_2 surface. Three desorption peaks were detected between 35 and 600°C. The low temperature desorption peak (up to 100°C) was ascribed to molecular hydrogen adsorbed on the surface. The next hydrogen desorption up to 200 °C corresponds to dissociated hydrogen adsorbed on the metal surface, and the high temperature desorption peaks (up to 450°C) correspond to hybrids formation with a very strong interaction between metal and hydrogen. No spillover species were observed (desorption between 700 and 800°C). In order to determine the oxidation state of Pt, XPS analysis was performed. After reduction, the sample was fully reduced with binding energies of the Pt $4f_{7/2}$ and Pt $4f_{5/2}$ levels of 71 and 74.5 eV, [18] respectively (Figure 2). The XPS analysis also confirmed that nitrate and chlorine ions used during the synthesis of the sample are fully removed from the surface.

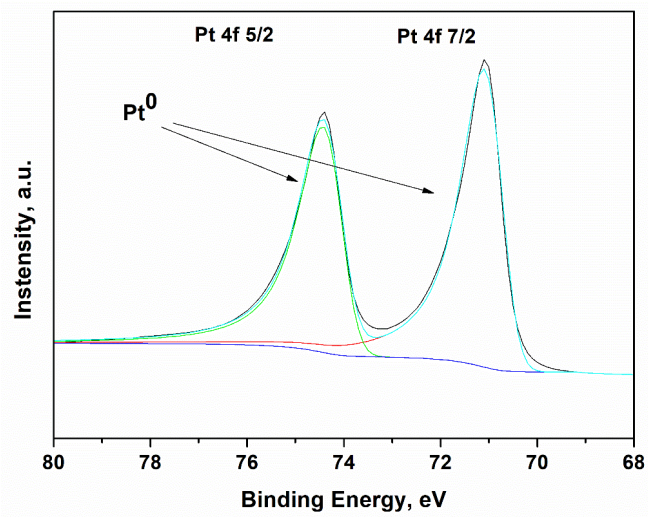

Figure 2. XPS spectra in the Pt 4f region for the reduced Pt/SiO_2 nanozyme catalyst.

Figure 3 shows the catalytic results obtained in the oxidative deamination of HMFA with the reaction pathway in Figure 4. After 24 h of reaction, from an initial quantity of 10 mmol, 3.25 mmol of HMFA were consumed to give 0.76 mmol of AMFA and 0.12 mmol of AMFC thought two sequential oxidation steps. However, 0.96 mmol HMF were also observed. In addition, as HMF oxidation products, 0.81 mmol AFCA and 0.59 mmol DCAF were also detected.

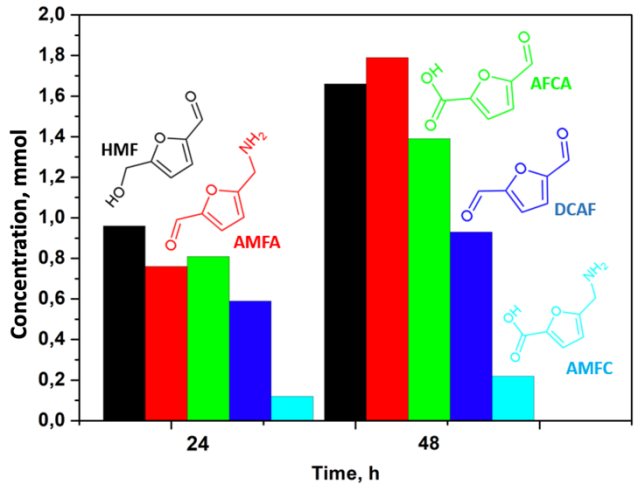

Figure 3. Product concentrations measured by high performance liquid chromatography with diode array detection (HPLC-DAD) after 24 and 48 h using Pt/SiO_2 nanozyme in a sodium phosphate buffer (pH 8). The conversion of HMFA is presented in Table 1.

These results are amplified after 48h of reaction: additional 2.75 mmol of HMFA were consumed, giving a total HMFA consumption of 6 mmol. Between 24 h and 48 h of reaction, AMFA production increased from 0.76 mmol to 1.79 mmol, while that more modest of AMFC increased from 0.12 mmol to 0.22 mmol. The amount of HMF and its oxidation products, on the other hand, was much more significant. During the last 24 h of reaction, the HMF quantity increased from 0.96 mmol to 1.66 mmol, while the amount of AFCA increased from 0.81 to 1.39 mmol, and that of DCAF from 0.59 to 0.93 mmol. Despite the significant amount of AMFA formed (1.79 mmol), the concentration of AMFC did not change significantly (0.10 mmol during 24 h), suggesting that AMFA plays an important role in the mechanism of DCAF formation.

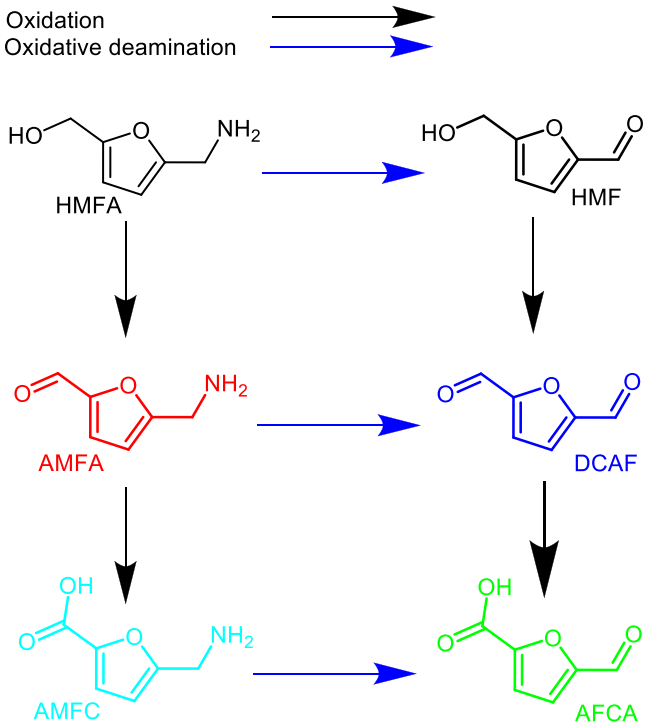

Figure 4. Schematic representation of reaction pathways studied in this work.

To confirm the deaminase mimic activity of Pt/SiO2, tests on oxidative deamination of l-glutamic acid at 60 °C and different pH were also performed. In presence of the nanozyme, the deamination extent slightly increased with the pH, with 0.44 , 0.49 and 0.75 mmol of product formation after 24h, for pH 8, 9 and 10 respectively (Table 1). l-pyroglutamic acid formation started from pH 9 under these conditions. In the absence of Pt/SiO2 (blank experiment), glutamic acid was fully converted to its cyclic form: l-pyroglutamic acid was formed, without any deamination, and the l-pyroglutamic formation extent followed the pH increase. As a bridge between homogeneous and heterogeneous catalysis, nanoscale metal particles have received renewed attention in catalysis [19-21]. Accordingly, an effective size control of the metal nanoparticles is important in order to precisely investigate their novel catalytic properties. Among the platinum group metals, the preparation of Pt nanoparticles has been extensively studied [22]. Colloidal metal particles are of interest because of their use as catalysts. Very often, the catalytic activity depends on the size and the shape of the metallic nanoparticles actually playing the role of the active phase, and the control of such critical parameters is essential. El-Sayed et al. [23] have prepared platinum nanoparticles by H2 reduction of K2PtCl4 in water at room temperature. Sodium polyacrylate was used as the protective agent. The shapes and sizes of the prepared platinum nanoparticles were controlled by tuning the ratio of the capping polymer concentration to the platinum ions concentration.

Table 1. Catalytic results obtained during oxidative deamination of HMFA and glutamic acid on Pt/SiO_2 nanozyme.

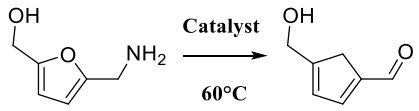

Time (h)	**Substrate and products concentrations (mmol)** [a] [b]					
	HMFA	HMF	AMFA	AFCA	DCAF	AMFC
0	10	0	0	0	0	0
24	6.74	0.96	0.76	0.81	0.59	0.12
48	4.0	1.66	1.79	1.39	0.93	0.22

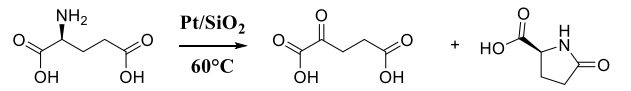

(*L*)-Glutamic Acid Acid alpha-ketoglutaric (*L*)-pyroglutamate

pH	**Substrate and products concentrations (mmol)** [a]					
	Glutamic acid		*α*-ketoglutaric acid		*L*-pyroglutamate	
	Pt/SiO_2	BT[c]	Pt/SiO_2	BT[c]	Pt/SiO_2	BT[c]
8	9.17	10	0.44	0	0	0

9	9.20	9.5	0.49	0	0	0.5
10	7.96	9.0	0.75	0	0.81	1.0

[a] Carbon balance was higher than 96% in all cases. [b] blank tests (BT) performed without catalyst showed any activity. No conversion of HMFA was observed nor products formation. [c] blank tests (BT) performed without catalyst

The distribution of particle size strongly depends on the polymer/platinum concentration ratios. Ingelsten *et al.* [24] have examined the effect of the surfactant type and of the temperature of synthesis on the kinetics of the formation of platinum nanoparticles by chemical reduction of $PtCl^{2-}$. Platinum nanoparticles with an average diameter of 5 nm could be prepared by reduction of H_2PtCl_6 with sodium borohydride in the presence of several surfactants. Rioux [25] has prepared platinum nanoparticles of well-defined shapes using chemical reduction of H_2PtCl_6 in ethylene glycol in the presence of PVP. The shapes of the nanoparticles were controlled by adding silver nitrate to the reactant solution. Addition of increasing amounts of $AgNO_3$ into the reactant solution led to the formation of cubic, cubo-octahedral and octahedral platinum nanoparticles.

In the present work the Pt/SiO_2 nanozyme was successfully synthetized by the precipitation method, which is by far the easiest way of synthesis. Moreover, the use of standard commercial precursors in the absence of a costly organic protective agent would favor perspectives of industrial up scaling. The results of the structural and chemical analyses confirmed that very small metallic Pt nanoparticles were obtained. This is crucial for the study of the catalytic properties of this nanozyme. Indeed, it is generally admitted that small metallic nanoparticles exhibit improved catalytic activity due to the combination of large proportions of high-energy surface atoms. It is also necessary to obtain sharp distribution of the sizes. Figure 3 and Table 1 strongly indicated that the Pt/SiO_2 nanozyme promotes the oxidative deamination reaction pathway. Indeed, oxidation of the amine function to the imine function would increase the electrophilic character of the alpha carbon of this function. The formation of HMF is favored because of the resulting aromaticity both of the intermediate in the imine form and of the various possible mesomeric forms of HMF, greatly increasing the stability of the molecule. To discuss the oxidation and deamination mechanisms, direct oxidation of HMF was also performed using the Pt/SiO_2 nanozyme. The results confirmed that Pt nanoparticles possess also oxidase-like abilities. The oxidation of alcohols and aldehydes in the liquid phase have been already extensively studied. In the case of HMF oxidation, two different pathways can occur as reported earlier [26-28]. The carbonyl group can be firstly oxidized to an acid group forming *5*-hydroxymethyl-*2*-furancarboxylic acid (HMFCA). The second step will be then the oxidation of the aldehyde group to form *5*-formyl-*2*-furancaboxylic acid (AFCA). This is the as called first pathway. The second one starts with the oxidation of the alcohol group to carbonyl group to form *2*,*5*-diformylfuran (DCAF). In the second step it is then oxidized to acid group. *5*-formyl-*2*-furancaboxylic acid (AFCA) is formed in this case. FDCA is the final product formed by the oxidation of carbonyl group of AFCA (pathway 2). It was reported that the nature of the metal can orient the reaction to a specific pathway. The presence of a gold favors the first pathway under basic conditions [29]. It was clearly showed that the alcohol group oxidation is the rate-determining step (HMFCA is formed). The formation of HMFCA was observed by Casanova *et al.* working with Au/CeO_2 and Au/TiO_2 catalysts under high pH conditions [30-31]. Moreover, the HMFCA was the only intermediate detected. The authors concluded that it could be due to the rapid conversion of AFCA to FDCA. Generally speaking, high pH favors the formation of HMFCA because of the fast hydration to a geminal diol.

The consecutive step of the geminal diol hydride elimination to acid is favored by the $^{-}$OH adsorbed on the metal [32]. The recent studies on the mechanisms using an isotope-labeling methodology were reported [33]. It was shown, that the oxygen plays a triple role: i) remove electrons from the metal surface, ii) oxidize metal–hydride bonds, and iii) regenerate the hydroxide ions. Accordingly, the four oxygen atoms incorporated to the FDCA molecule originated from water. It is generally admitted that in the case of Pt, the reaction pass through the DCAF formation (second pathway). Firstly, the dialdehyde (DCAF) is formed and then it is oxidized to AFCA and to FDCA. This is in full agreement with the observations in the present study. The concentration of DCAF was always lower than that of AFCA. In addition, the presence of the HMFCA intermediate was not observed, which confirms that the second pathway is favored in the case of Pt nanoparticles.

Concerning the oxidative deamination reaction mechanism, the first step is the adsorption of the amine group on the metal surface (Figure SI14). It is bounded through the interaction between nitrogen and the proton abstracted during the aldehyde oxidation reaction as described above. The second hydrogen bond with the hydrogen from amine group and metal surface is also formed. Next, the water molecule is added to form the carbinolamine. This intermediate is then hydrolyzed to release the keto compound. Similar mechanism was recently proposed by Tang et al. [34] with water playing the role of oxidant.

These two reactions seem to occur simultaneously, as the yield of the formed AMFA and HMF are comparable during the whole the reaction. No adsorption is observed when SiO_2 alone is used. It could be concluded that the adsorption mode of the substrate is the crucial step. When adsorbed by amine group the oxidative deamination occurred. In the case of alcohol or aldehyde group adsorption, the oxidation products are favored.

Conclusion

As a conclusion, we have outlined the use of nanozymes acting as a deaminase mimic. We demonstrated that a Pt/SiO_2 nanozyme, composed of finely dispersed platinum nanoparticles stabilized on the silica surface, are active and selective in the liquid phase oxidative deamination of HMFA and glutamic acid. This work gives also insight in the oxidative deamination reaction pathway using Pt nanoparticles. We showed that in the case of HMFA, the deamination and oxidation steps occurred at the same time forming similar quantities of HMF and AMFA. In addition, the catalyst also exhibited activity in different conditions of pH (8-10). The use of available materials (Pt and SiO_2) is also very interesting for industrial applications.

Experimental Section

Pt/SiO_2 catalyst was synthetized as follows: adequate quantities of $Pt(NH_3)_4Cl_2$ and $Pt(NH_3)_4(OH)_2$ (ratio 1:1) were dissolved in deionized water. Silica (Degussa; specific surface area: 203 $m^2.g^{-1}$) was then added and the pH of the reactant mixture was maintained at 8.9. The mixture was mixed for 1h at room temperature, filtered, and washed with hot water to remove all the Cl^- ions. The solid was then dried at 105 °C for 2h and reduced with pure hydrogen at 420°C for 4h (2°C.min^{-1} and 50cm^3.min^{-1} H_2). The final Pt loading was 6.3 wt.%, as determined by ICP analysis. The surface area of the catalyst was 185 m^2/g as determined by N_2 physisorption isotherms at liquid nitrogen temperature carried out on a TriStar II Plus gas adsorption analyzer (Micromeritics) after activation at 150 °C in vacuum overnight. The specific surface area was evaluated with the Brunauer-Emmett-Teller (BET) model over the

range P/P0 = 0.05 – 0.30. The surface was not significantly affected by the Pt deposition (9 % decrease was observed).

The ICP-OES (Inductively Coupled Plasma Optical Emission Spectrometry) analysis was performed using Agilent 720-ES ICP-OES equipment combined with Vulcan 42S automated digestion system.

Transmission Electron Microscopy (TEM) images were recorded placing a drop of the particle's dispersion in *iso*propanol over a carbon film supported on a cooper grid. FEI Tecnai microscope was used for the recording of the images. We observed the presence of platinum particles in the range 0.9 to 4 nm. About 70 per cent of the particles are less than or equal to 2 nm. This agreement leads to the conclusion that the platinum particles have a dispersion close to 60%. More than 600 particles were used for the distribution size studies. It was performed using Image J software.

X-ray Photoelectron Spectroscopy (XPS) analysis was performed on an XPS Kratos, Axis UltraDLD "2009" with monochromatic Al Kα ($h\nu$=1486.6 eV) radiation as the excitation source and equipped with high-performance hemispheric analyzer. Calibration of the binding energies was performed using the carbon C 1s reference at 284.8 eV.

Hydrogen chemisorption on the reduced sample was performed using a mixture of H_2/Ar (100 ppm of H_2). 0.1 g of sample were placed in a quartz reactor and treated in a H_2 flow (flow rate of 100 cm^3min^{-1}) at 300 °C for 2 h. After activation, the sample was purged in a flow of argon at 300°C for 1. It was then cooled to 35 °C in a flow of Ar. Hydrogen adsorption was then carried out at 35 °C in a flow of H_2/Ar (100 $cm^{-3}.min^{-1}$; 100 ppm of H_2 in Ar). The consumption of hydrogen was measured each 2 min with a thermal conductivity detector (TCD) in an Agilent G2890A series MicroGCs gas chromatograph equipped with molecular sieves as a column (8 m), operated at 250°C.

Hydrogen temperature-programmed desorption (H_2-TPD) was performed under argon flow directly after hydrogen adsorption. The sample was purged with argon at 35°C for 1h. The sample was then heated at a rate of 5°C.min^{-1} to 800°C under argon flow (50cm^3.min^{-1}). The quantity of desorbed hydrogen was measured each 2 min with a thermal conductivity detector (TCD) in an Agilent G2890A series MicroGCs gas chromatograph operating at 250°C.

Oxidative deamination of the selected substrate (HMFA or glutamic acid) was performed in a 2 mL GC vial. 2 mg of solid catalyst were added to 1 mL of a 10 mM substrate solution in 100 mM sodium phosphate buffer (pH 7, 8 or 9) in ultra-pure water. The vials were incubated at 60 °C in a stove and stirred using a rotative agitator (Tube Revolver, Thermoscientific, USA) at 22 rpm, with an angle of 45° compared to the rotation axis to maintain good homogeneity in the reaction mixtures comprising the solid heterogeneous catalyst. The temperature was chosen in order to study the compatibility between heterogeneous and enzymatic catalysts. A blank reaction was performed without the addition of a catalyst. To follow the product formation, 50 µL aliquots were collected after 24 and 48h before analysis by HPLC-DAD (*vide supra*). For HMFA conversion experiments, the reaction products' analyses were performed on an Ultra-fast HPLC-DAD-MS–LCMS-2020 (Shimadzu, Japan), using a Brownlee Spheri-5 RP-18 (4.6 x 250 mm) cartridge column. Injection volumes of 10 µL were used for all the samples. The water and acetonitrile elution phases contained 0.1 % trifluoroacetic acid (TFA). Elution was carried out at 0.5 mL.min^{-1}, with a 30 °C oven temperature for the column. The elution profile was as follows: 15 min of 100 % water phase, followed by the progressive shifting of the water phase toward 100 % acetonitrile phase in 2 min. The 100 % acetonitrile phase was then held for 2 min and then shifted again to 100 % water phase in 2 min. The 100 % water phase was then held until the end of the run (4 min more), with a total run time of 25 min

necessary to equilibrate the column and reach a stable pressure for the next injection. The products were detected at three different wavelengths, namely 215, 245, and 280 nm. For analyzing/quantifying the products of glutamic acid conversion experiments, ^{1}H and ^{13}C NMR spectra were recorded at 25 °C using a Bruker Advance 300 spectrometer. The coupling constants were measured in Hertz (Hz) and multiplicities for ^{1}H NMR coupling were presented as *s* (singlet), *d* (doublet), *t* (triplet), and *m* (multiple). The chemical shift is presented relatively to the sodium trimethylsilyl propanoate taken as a reference. NMR data are reported in Supplementary Information.

Acknowledgements
The HPLC-MS experiments were performed on the REALCAT platform funded by a French governmental subsidy managed by the French National Research Agency (ANR) within the frame of the "Future Investments' program (ANR-11- EQPX-0037). The Hauts-de-France region, FEDER, Ecole Centrale de Lille, and Centrale Initiatives Foundation are also warmly acknowledged for their financial contributions to the acquisition of REALCAT platform equipment. Finally, this study was sup-ported by the French government through the Programme Investissement d'Avenir (I-SITE ULNE / ANR-16-IDEX-0004 ULNE) managed by the Agence Nationale de la Recherche. I-SITE and Métropole Européen de Lille are also acknowledged (RECABIO and CatBioInnov project). Chevreul Institute (FR 2638), Ministère de l'Enseignement Supérieur, de la Recherche et de l'Innovation, Région Hauts-de-France and FEDER are acknowledged for supporting and funding partially this work.

Keywords: oxidative deamination • nanozymes • Pt nanoparticles • catalysis • HMF

[1] B.H. Asghar, H.M. Altass, A. Fawzy, *J. Environ. Chem. Eng*. **2016**, *4*, 617–623.
[2] A. Fawzy, I.A. Zaafarany, F. Tirkistani, I. Althagafi, J. Alfahemi, *J. Multidisc. Eng. Sci. Technol*. **2015**, *2*, 1038–1045.
[3] T.P. Jose, S.T. Nandibewoor, S.M. Tuwar, *E J. Chem*. **2005**, *2*, 75–85
[4] A. Goel, S. Sharma, *Transition Met. Chem*. **2010**, *35*, 549–554.
[5] A. Fawzy, I.A. Zaafarany, *Chem. Sci. Rev. Lett*. **2015**, *4*, 608–618.
[6] G. Golime, G. Bogonda, H. Kim, K. Oh, Y. Sun, X. Wang, K. Liang, Z. Jiang. *ACS Catal*. **2018**, *8*, 4986−4990.
[7] Y. Huang, J. Ren, X. Qu, *Chem. Rev.* **2019**, *119*, 4357−4412.
[8] L. Gao, J. Zhuang, L. Nie, J. Zhang, Y. Zhang, N. Gu, T. Wang, J. Feng, D. Yang, S. Perrett, X. Yan. *Nat. Nanotechnol*., **2007**, *2*, 577−583.
[9] X. Zheng, Q. Liu, C. Jing, Y. Li, D. Li, W. Luo, Y. Wen, Y. He, Q. Huang, Y. Long, Ch. Fan. *Angew. Chem. Int. Ed*. **2011**, *50*, 11994−11998.
[10] Y. Hu, H. Cheng, X. Zhao, J. Wu, F. Muhammad, S. Lin, J. He, L. Zhou, C. Zhang, Y. Deng, P. Wang, Z. Zhou, Sh. Nie, H. Wei, *ACS Nano* **2017**, *11*, 5558−5566.
[11] W. Luo, C. Zhu, S. Su, D. Li, Y. He, Q. Huang, C. Fan, *ACS Nano* **2010**, *4*, 7451−7458.
[12] Y. Li, X. He, J. Yin, Y. Ma, P. Zhang, J. Li, Y. Ding, J. Zhang, Y. Zhao, Z. Chai, Z. Zhang. *Angew. Chem., Int. Ed.* **2015**, *54*, 1832−1835.
[13] Y. Huang, Z. Liu, C. Liu, E. Ju, Y. Zhang, J. Ren, X. Qu. *Angew. Chem. Int. Ed.* **2016**, *55*, 6646−6650.
[14] R. Wojcieszak, I. Cuccovia, M. Silva, L. Rossi, *J. Mol. Catal. A: Chem*., **2016**, *422*, 35-42.
[15] A. Vernekar, D. Sinha, S. Srivastava, P. Paramasivam, P. D'Silva, G. Mugesh, *Nat. Commun*. **2014**, *5*, 5301.

[16] F. De Schouwer, T. Cuypers, L. Claesa, D.E. De Vos, *Green Chem*., **2017**, *19*, 1866–1876.
[17] Y. Wu, J. Shi, Sh. Mei, H. A. Katimba, Y. Sun, X. Wang, K. Liang, Z. Jiang. *ACS Catal*. **2018**, *8*, 4986−4990.
[18] V. Baldovino-Medrano, G. Pollefeyt, V. Bliznuk, I. Van Driessche, E. Gaigneaux, P. Ruiz, R. Wojcieszak, *ChemCatChem*, **2016**, *8*, 1157-1166.
[19] S. Panigrahi, S. Kundu, S.K. Ghosh, S. Nath, T. Pal, *J. Nanopart. Res*. **2004**, *6*, 411- 414.
[20] M. Bettahar, R. Wojcieszak, S. Monteverdi, *J. Coll. Inter. Sci*. **2009**, *332*, 416-424
[21] G. Hutchings. Heterogeneous Gold Catalysis. *ACS Cent. Sci*. **2018**, *4*, 1095-1101.
[22] P. de Souza, L. Silvester, A. da Silva, C. Fernandes, T. Rodrigues, S. Paul, P. Camargo, R. Wojcieszak. *Catalysts*, **2019**, *9*, 132.
[23] T. Ahmadi, Z. Wang, T. Green, A. Henglein, M. El-Sayed, *Science* **1996**, *272*, 1924-1925.
[24] H. Ingelsten, R. Bagwe, A. Palmqvist, M. Skoglundh, Ch. Svanberg, K. Holmberg, D. Shah, *J. Coll. Inter. Sci*. **2001**, *241*, 104-111.
[25] R.M. Rioux, H. Song, M. Grass, S. Habas, K. Niesz, J.D. Hoefelmeyer, P. Yang, G.A. Somorjai, *Topics in Catalysis* **2006**, *39*, 167-174.
[26] S. Davis, B. Zope, R. Davis, *Green Chem*. **2012**, *14*, 143-1473.
[27] C.P. Ferraz, M. Zieliński, M. Pietrowski, S. Heyte, F. Dumeignil, L. Rossi, R. Wojcieszak. *ACS Sust. Chem. Eng*. **2018**, *6*, 16332-16340.
[28] R. Wojcieszak, C.P. Ferraz, J. Sha, S. Houda, L. Rossi, S. Paul. *Catalysts*, **2017**, *7*, 352.
[29] M. Lilga, R. Hallen, M. Gray, *Top. Catal.* **2010**, *53*, 1264–1269.
[30] O. Casanova, S. Iborra, A. Corma, *ChemSusChem* **2009**, *2*, 1138–1144.
[31] O. Casanova, S. Iborra, A. Corma, *J. Catal*. **2009**, *265*, 109–116.
[32] S. Davis, M. Ide, R. Davis, *Green Chem*. **2013**, *15*, 17–45.
[33] B. Zope, D. Hibbitts, M. Neurock, R. Davis, *Science*, **2010**, *330*, 74–78.
[34] S. Tang, M. Rauch, M. Montag, Y. Diskin-Posner, Y. Ben David, D. Milstein, *JACS*, **2020**, *142*, 20875-20882